Preprints of the 21st IFAC World Congress (Virtual)
Berlin, Germany, July 12-17, 2020

FDI Study for a Wave Energy Converter by Structural Analysis ⋆

Alejandro G. González E. * **Cristina Verde** *
Paul Maya-Ortiz **

* *Instituto de Ingeniería, Universidad Nacional Autónoma de México, Circuito Exterior S/N, 04510, Mexico City (agonzaleze@iingen.unam.mx; verde@unam.mx)*
** *Facultad de Ingeniería, Universidad Nacional Autónoma de México, Circuito Exterior S/N, 04510, Mexico City (paulm@unam.mx)*

Abstract: This paper presents a fault diagnosis study for a wave energy converter by using structural analysis (SA) as the main tool. An Archimedes wave swing-based converter is considered as a case study with a detailed model taken from a real case. Thus, one looks for robust residuals for the irregular wave effects and sensitivity to fault detection. The faults considered for the device are as follows: central tank perforation, brakes damage, position and speed sensor faults, as well as an actuator fault. The transient response of the residuals to these faults is simulated by MATLAB/Simulink and demonstrates the potentiality of the analysis.

Keywords: Structural analysis and residual evaluation methods, computational methods for FDI, process control applications

1. INTRODUCTION

Ocean wave energy has a significant potential for contributing to the energy targets of clean and renewable energy because it has a generation capability over 26,000 TWh per year (Mork et al., 2010). Since there is no noticeable consensus about the most efficient mechanism for ocean waves (Magagna and Uihlein, 2015), a wide variety of different devices are being designed, tested and developed, as reported by Pecher and Kofoed (2017).

Point absorbers are an important class of wave energy converters (WECs). Their operation principle is to convert mechanical energy from a floater motion produced by incident waves to electrical energy. This is done in many different ways, for example, by means of gear trains or hydraulic systems to provide fluid flow to a turbine connected to a rotary generator or, in contrast, by using a direct drive linear generator (Drew et al., 2009). The Archimedes wave swing (AWS) concept is included in this class of WECs. An AWS prototype reported by Prado et al. (2006) is considered as a good reference since it can provide power generation with peak values around 2 MW.

Control systems for WECs are designed to maximize energy extraction by following criteria like those presented by Falnes (2002), and by providing a steady energy supply despite the irregularity of sea waves as reported by Penalba et al. (2017).

Since the installation and maintenance of WECs are complicated and expensive tasks and because the oxidation caused by sea water is a frequent issue, automatic fault diagnosis and monitoring systems are important security requirements to consider. Some previous studies related to such topics in WECs are the following: Chandrasekaran and Raghavi (2015) developed a failure mode and effect analysis for a prototype that includes lever arm and gear boxes in addition to the floating buoy, without involving the physical parameters from the beginning. Furthermore, Ambühl et al. (2015) studied maintenance strategies applied to the Wavestar WEC and then evaluated the influences of different parameters, such as failure rate, inspection quality for the overall costs and the number of repairs needed during its lifetime. Johanson et al. (2019) designed a reference architecture for WEC condition monitoring and presented a prototype implementation under proposed guidelines.

Note that there are no previously reported FDI analyses over WECs considering their mathematical model, as it is presented in this work. The considered case study is a WEC based on the AWS prototype presented by Prado et al. (2006). This system is placed on the sea floor, and the floater is a 4×10^5 kg lid that covers a 40 m high 3000 m^3 capacity air filled tank, enclosed by a strengthening structure that includes adjustable brakes attached to the floater that provide necessary damping under operating conditions. Electrical energy is obtained from a *linear permanent magnet generator* (LPMG) placed inside the air filled tank. In addition, water pumps and auxiliary tanks are included for adjusting the mean value of the air pressure inside the tank and the oscillation of the floater. Since this converter is under extreme conditions on the sea bottom, supervision and maintenance are fundamental tasks from a practical and safety point of view.

There are different approaches for managing the FDI problem from a mathematical model. Some examples are

⋆ This research is supported by the UNAM program for Master of Science and Doctorate studies in engineering, the UNAM-PAPIIT program IT100519DGPA-UNAM, CEMIE-Océano, and CONACyT.

methods based on bond graphs as have been reported by Liu and Yu (2017) to diagnose faults in an electromechanical actuator, as well as structural analysis (SA) that has been used by Sundström et al. (2013) to diagnose faults in a hybrid vehicle. This last approach is the one considered in this work since it provides detectability and isolability conditions that are independent of the values of the parameters that define the mathematical model. Therefore, it can be applied for complex systems such as the one here considered.

This study considers damages associated with the mechanical parts of the system. They are a perforation in the tank, failure in the dampers, faults in the position and speed sensors of the floater, as well as in the LPMG.

The main contribution is an FDI study for a WEC under a model-based approach, which has not been previously considered for such a system. A selection of feasible ARRs is included, where the starting point is the minimal structurally overdetermined sets generated by the algorithm of Krysander et al. (2007) such that the ARRs are robust in presence of the irregular sea wave. In addition, by processing the transient response to faults of some residuals, the isolation of some structurally non-isolable faults is achieved.

2. STRUCTURAL ANALYSIS PRELIMINARIES

Structural analysis (SA) (Staroswiecki et al., 2000) is a technique that provides general conditions for fault detectability and isolability for nonlinear systems described by lumped-parameter models. Under this approach, the constraints $\mathcal{C}$ (i.e., algebraic and differential equations) and the variables, $\mathcal{Z} = \mathcal{K} \cup \mathcal{X}$, are linked by a bipartite graph $\mathcal{G} = \{\mathcal{C}, \mathcal{Z}\}$, where $\mathcal{K} = \mathcal{U} \cup \mathcal{Y}$ denotes the known variables subset, which is conformed by inputs $\mathcal{U}$ and measurements $\mathcal{Y}$. Furthermore, $\mathcal{X}$ denotes the unknown variables, and $\mathcal{G}$ can be represented as an incidence matrix IM. Moreover, let $\mathcal{F}$ be the set of considered faults. A violation of $c_i \in \mathcal{C}$ is considered to be caused by $f_j \in \mathcal{F}$ (Blanke et al., 2016).

2.1 Canonical Decomposition of a Bipartite Graph

By using the decomposition from Dulmage and Mendelsohn (1958) of the IM of the system with only the set $\mathcal{X}$, one can obtain the graph $\mathcal{G}^+ = \{\mathcal{C}^+, \mathcal{X}^+\}$ with more constraints than unknown variables, which is the only useful subgraph for fault diagnosis. This is because if $f_i \in \mathcal{F}$ affects $c_j \in \mathcal{C}^+$ associated variables may be obtained from $\{\mathcal{C}^+ \backslash \{c_j\}, \mathcal{X}^+\}$. If $\mathcal{G} = \mathcal{G}^+$, the graph is called *proper structurally overconstrained* (PSO), and its *structural redundancy measure* is given by $\varrho(\mathcal{G}^+) = |\mathcal{C}^+| - |\mathcal{X}^+|$.

2.2 Minimal Structurally Overdetermined Sets

Minimal structurally overdetermined sets (MSOs) are subsets of $\mathcal{G}^+$ such that $\varrho\{MSO_i\{\mathcal{C}_i, \mathcal{X}_i\}\} = 1$. An MSO allows building an *analytical redundancy relation* (ARR) by choosing a constraint as a *consistency relation* in order to test computed results from the remaining just-constrained subset. An algorithm developed by Krysander et al. (2007) can be used to find *MSO candidates* in $\mathcal{G}^+$.

Let $c_r \in \mathcal{C}_i$ be chosen as the consistency relation. If the equation system represented by $\{\mathcal{C}_i \backslash \{c_r\}, \mathcal{X}_i\}$ has a unique solution set $\mathcal{X}_i^S$, then c_r can be used to define an ARR. A procedure for determining $\mathcal{X}_i^S$ can be summarized in a *computation sequence* (Zhang and Rizzoni, 2014).

2.3 Structural Detectability and Isolability

The following conditions must hold for structural detectability and isolability of a fault f_j (Blanke et al., 2016):

- *Structural Detectability:* A fault $f_j \in \mathcal{F}$ that causes a violation of $c_i \in \mathcal{C}$ is *structurally detectable* iff it has a nonzero Boolean signature in some residual r.
- *Structural Isolability:* A fault $f_j \in \mathcal{F}$ that causes a violation of $c_i \in \mathcal{C}$ is *structurally isolable* iff it has a unique fault signature (i.e., the set of residuals sensitive to f_j is unique).

3. WAVE ENERGY CONVERTER

This section describes the selected WEC operation principle and model. Constraints to be used in the structural analysis and considered faults are also established.

3.1 WEC Operation

The AWS is basically a submerged WEC composed of an air-filled chamber (central tank) fixed to the sea bottom and covered by a lid (floater) that heaves according to waves on the surface and enclosed air expansion (Prado et al., 2006). This operation principle is depicted in Figure 1. Related variables are defined in Table 1.

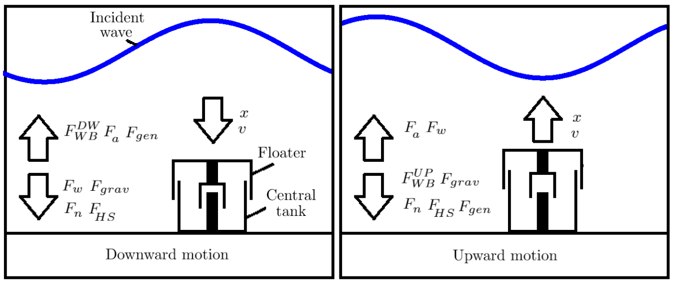

Fig. 1. WEC Operation principle

The water level inside the central tank is adjusted in order to tune the natural oscillation frequency of the floater motion ω_n. Wave energy conversion efficiency is maximized by setting ω_n to match the incident sea waves frequency (Falnes, 2002). Because the central tank water level adjustment is a slow process, average wave frequencies are used (Prado et al., 2006).

For system safety under diverse operating conditions, water brakes are included in the structure for providing additional damping. These devices are composed of a cylinder tube attached to the floater that encloses another cylinder attached to the strengthening structure. The provided friction is considerably greater when floater motion pushes out water enclosed between both tubes, so isolated damper systems are required for the upwards and downwards motion of the floater. Each brake is tuned by adjusting a valve aperture in its fixed tube (Beirao, 2007). The importance

Table 1. WEC model variables and parameters

x	Floater position	F_k	Total stiffness force over the floater
v	Floater speed	F_b	Total damping force over the floater
F_w	Incident wave force	F_{WB}^{UP}	Upper water brake friction force
F_{grav}	Floater weight	F_{WB}^{DW}	Lower water brake friction force
F_r	Radiation force. $F_r = -m_{add}\dot{v}$	m_f	Floater mass
p_{amb}	Atmospheric pressure	m_{add}	Floater added mass
η_T	Tide level	m_t	Floater total mass $m_t = m_f + m_{add}$
i_{abc}^{Grid}	Grid three-phase currents	d_f	Floater depth at x = 0
v_{abc}^{Grid}	Grid three-phase voltages	S_f	Floater and central tank base area
i_{abc}	LPMG stator three-phase currents	V_{a0}	Central tank air volume at $h_w = 0$, $x = 0$
v_{abc}	LPMG stator three-phase voltages	S_n	Nitrogen cylinder base area
F_{gen}	LPMG force	V_{n0}	Nitrogen cylinder gas volume at $x = 0$
F_{gen}^*	Desired LPMG force	γ	Heat capacity ratio
u_{gen}	LPMG control law (applied through v_{abc})	ρ	Sea water density
β_{WB}	Water brakes coefficient	g	Earth gravitational constant
h_w	Water level inside central tank	y_1	Measurement of x
h_w^*	h_w desired value	y_2	Measurement of v
p_a	Air pressure inside central tank	y_3	Measurement of an LPMG stator current
F_a	p_a force over the floater	y_4	Measurement of F_w
p_n	Gas pressure inside nitrogen cylinder	f_1	Position sensor multiplicative fault
F_n	p_n force over the floater	f_2	Speed sensor multiplicative fault
p_{HS}	Hydrostatic pressure over the floater	f_3	LPMG fault
F_{HS}	p_{HS} force over the floater	f_4, f_5	Upper and lower water brakes faults
x^0	Floater equilibrium position	f_6	Central tank water level fault
p_a^0	Central tank air pressure at $x = x^0$		

of these brakes comes from the great forces on the sea bottom produced by incident waves, which would cause several impacts between the floater and the structure.

Electrical energy is obtained with a linear permanent magnet generator (LPMG) located inside the central tank. Its traslator is attached to the floater, and its stator is connected to the grid through a back-to-back converter.

3.2 WEC Model

Model equations of the considered WEC are presented. Constraints used for the SA are denoted by $c_i \in \mathcal{C}$, $m_i \in \mathcal{C}$ for measurements related constraints, and $d_i \in \mathcal{C}$ for differential constraints. The interconnection of the subsystems is given in Figure 2.

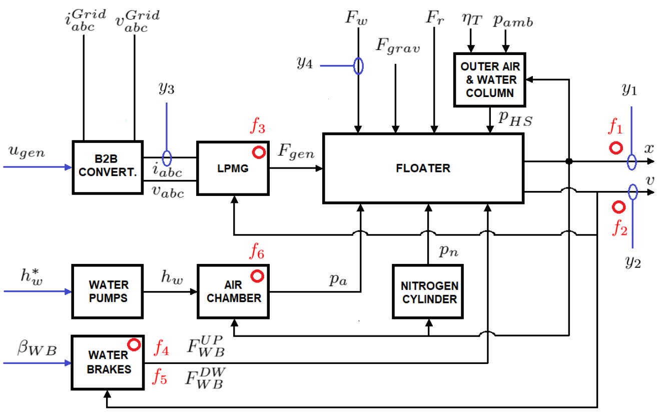

Fig. 2. WEC block diagram. Faults and known signals are highlighted in red and blue respectively.

By using the variables and parameters in Table 1, the floater dynamics for $|x| < 4.5\ m$ and $|v| < 2.2\ \frac{m}{s}$ are

$$c_1: \quad \dot{x} = v, \tag{1}$$

$$c_2: \quad \dot{v} = \frac{1}{m_t}\left\{F_b + F_k + F_{gen} + F_w\right\}, \tag{2}$$

$$d_1: \quad \dot{x} = \frac{d}{dt}x, \quad d_2: \quad \dot{v} = \frac{d}{dt}v, \tag{3}$$

where the measurements of the position and speed could be affected by faults f_1 and f_2, as follows:

$$m_1: \quad y_1 = (1 + f_1)x, \tag{4}$$

$$m_2: \quad y_2 = (1 + f_2)v. \tag{5}$$

In addition, the forces over the floater are given by the following.

- *F_k: Total Stiffness Force*

This force depends on diverse pressures and the weight of the floater and is modeled by

$$c_3: \quad F_k = -S_f p_{HS} - S_n p_n + S_f p_a - m_f g, \tag{6}$$

$$c_4: \quad p_{HS} = [\rho g(d_f + \eta_T - x) + p_{amb}], \tag{7}$$

$$c_5: \quad p_n = p_n^0\left(\frac{V_n^0}{V_{n0} - S_n x}\right)^\gamma, \tag{8}$$

$$c_6: \quad p_a = p_a^0\left(\frac{V_a^0}{V_{a0} - S_f h_w + S_f x}\right)^\gamma, \tag{9}$$

where η_T, p_{amb} are constant known parameters, $\gamma = 1.4$ since adiabatic gas expansion is assumed, and h_w is the water level inside the central tank.

In the absence of sea waves, the floater equilibrium position x^0 is driven by p_a^0, p_n^0, p_{HS} as follows:

$$p_a^0 - \rho g(d_f + \eta_T - x^0) + p_{amb} - \frac{m_f g}{S_f} - \frac{S_n}{S_f}p_n^0 = 0, \tag{10}$$

where p_a^0 is adjusted in order to set the floater mean position. This is done by tuning the total water mass inside the system (central tank and auxiliary tanks), pumping sea water in or out of the auxiliary tanks. In addition, the natural frequency of the floater mainly depends on the water mass (air volume) inside the central tank since the air exchange between the central tank and the auxiliary tanks caused by floater motion is negligible (Beirao, 2007). Therefore, h_w is considered a constant fixed value h_w^*. Furthermore, h_w is tuned by pumping water to (from) the central tank from (to) auxiliary tanks. If a central tank perforation occurs, h_w changes. This effect is modeled by

$$c_7: \quad h_w = h_w^* + f_6, \tag{11}$$

where the difference in water level is modeled by f_6. Thus, a tank perforation modifies the average values of x and p_a. Since $p_a << p_{HS}$, it is considered that no air will escape because of an eventual perforation, so Eq. (9) remains valid under such circumstance.

- *F_b: Total Damping Force*

$$F_b = F_{br} + F_{drag} + F_{WB}^{UP} + F_{WB}^{DW}, \tag{12}$$

where F_{drag} is the drag force applied by the water on the floater and F_{br} is the force produced by the friction of the bearings, which are negligible compared with F_{WB}^{UP} and F_{WB}^{DW}. Under these conditions, F_b is reduced to

$$c_8: \quad F_b = F_{WB}^{UP} + F_{WB}^{DW}, \tag{13}$$

where the upper and lower water brakes actions are

$$c_9: \quad F_{WB}^{UP} = -\beta_{WB}(1 + f_4)v|v|H(v), \tag{14}$$

$$c_{10}: \quad F_{WB}^{DW} = -\beta_{WB}(1 + f_5)v|v|H(-v), \tag{15}$$

where $H(\cdot)$ is the Heaviside step function and f_4 and f_5 are faults over each brake.

- *F_{gen}: LPMG Force*

A control system for the LPMG to make it control floater movement thru F_{gen} is supposed. As the generator stator

Table 2. Dulmage-Mendelsohn decomposition of the incidence matrix of the WEC. Constraints related to faults under study are highlighted

	x	v	$\dot{x}$	$\dot{v}$	F_b	F_{WB}^{UP}	F_{WB}^{DW}	F_k	p_a	p_n	p_{HS}	h_w	F_{gen}	$\dot{\zeta}_{gen}$	ζ_{gen}	F_w
c_4	•										•					
c_1		•	•													
d_1	•		•													
d_2		•		•												
c_8					•	•	•									
c_9		•				•										
c_{10}		•					•									
c_2				•	•			•					•			•
c_6	•								•			•				
c_5	•									•						
c_3								•	•	•	•					
c_7												•				
c_{12}													•		•	
c_{11}														•	•	
d_3														•	•	
m_4																•
m_1	•															
m_2		•														
m_3	•												•			

circuit dynamics are faster than the floater motion and wave incidence, by considering a control system for the LPMG the obtained input-output dynamics are approximated by

$$c_{11}: \quad \dot{\zeta}_{gen} = \frac{1}{\tau_{gen}} \left\{-\zeta_{gen} + (1+f_3)F^*_{gen}\right\}, \tag{16}$$

$$c_{12}: \quad F_{gen} = \zeta_{gen}, \tag{17}$$

$$d_3: \quad \dot{\zeta}_{gen} = \frac{d}{dt}\zeta_{gen}, \tag{18}$$

where F^*_{gen} is the desired LPMG force, τ_{gen} is a time constant defined by the generator control system, ζ_{gen} is the approximated LPMG model state variable and f_3 is a fault over LPMG such as a permanent magnet degradation or components affected by rusting. Tracking of F^*_{gen} by F_{gen} is achieved by means of the control law u_{gen}. A detailed LPMG model is described by Wu et al. (2013).

Since the stator three-phase currents i_{abc} are directly measurable, the following constraint is also considered:

$$m_3: \quad y_3 = \varphi(F_{gen}, x), \tag{19}$$

from the $dq0$ reference frame where F_{gen} is proportional to i_q, which is related to i_{abc} by a Park-like transformation which depends on x (Wu et al., 2013). Therefore, y_3 represents the measurement of any three-phase current.

• F_w: *Incident Wave Force*
Incident waves are modeled by a JONSWAP spectrum approximation in this work. As the pressure on the top of the floater is measurable (Prado et al., 2006), one can estimate F_w and then

$$m_4: \quad y_4 = F_w. \tag{20}$$

4. WEC STRUCTURAL ANALYSIS

4.1 WEC Incidence Matrix

The cardinality of the sets that define the WEC bipartite graph $\mathcal{G}_{WEC}$ is given by $|\mathcal{X}| = 16$, $|\mathcal{K}| = 5$, $|\mathcal{C}| = 19$. Each of these sets and the considered faults are composed by

- Unknown variables: $\mathcal{X} = \{x, v, \dot{x}, \dot{v}, F_b, F_{WB}^{UP}, F_{WB}^{UP}, F_k, p_a, p_n, p_{HS}, h_w, F_{gen}, \zeta_{gen}, \dot{\zeta}_{gen}, F_w\}$,
- Known variables: $\mathcal{K} = \{y_1, y_2, y_3, y_4\} \cup \{F^*_{gen}\}$,
- Constraints: $\mathcal{C} = \{c_1, \ldots, c_{12}, m_1, \ldots, m_4, d_1, d_2, d_3\}$,
- Faults: $\mathcal{F} = \{f_1, \ldots, f_6\}$.

The DM decomposition of $\mathcal{G}_{WEC}$ through its incidence matrix given in Table 2 shows that the system is PSO.

4.2 Minimum Structurally Overconstrained Sets

The system structure is analyzed with the SaTool toolbox 2013 version (Wolf, 2013) for MATLAB. By selecting the option of the algorithm of Krysander et al. (2007), 11 MSOs were obtained. Relations between the faults and the MSOs are summarized in Table 3. Entries related to MSO_3 and MSO_9 are highlighted because they require computing variables from a non-bijective relation.

From these sets, it can be noticed that all the faults are structurally detectable and f_4, f_5, and f_6 are not structurally isolable.

Table 3. Obtained MSOs

	f_1	f_2	f_3	f_4	f_5	f_6
MSO_1	•		•			
MSO_2	•	•		•	•	•
MSO_3		•	•	•	•	•
MSO_4	•	•	•	•	•	•
MSO_5	•	•				
MSO_6		•	•			
MSO_7		•		•	•	•
MSO_8	•			•	•	•
MSO_9			•	•	•	•
MSO_{10}		•	•	•	•	•
MSO_{11}	•		•	•	•	•

By choosing MSOs 1 ,4, 5 for the implementation of the residual generators, the fault signature matrix shown in Table 4 is obtained. This selection allows obtaining different fault signatures for f_1, f_2, f_3 and the group $\{f_4, f_5, f_6\}$ composed of non-structurally isolable faults.

Table 4. WEC fault signature matrix

		f_1	f_2	f_3	f_4	f_5	f_6
r_1	MSO_1	•		•			
r_2	MSO_4	•	•	•	•	•	•
r_3	MSO_5	•	•				

4.3 Residual Generation

• r_1: By choosing c_{11} as the consistency relation, the computation sequence for r_1 is

$$CS_1 = \{(m_1, x), (m_3, F_{gen}), (c_{12}, \zeta_{gen})\}. \tag{21}$$

Thus, the obtained ARR are given by

$$\dot{\zeta}_{gen} = \frac{1}{\tau_{gen}} \left\{-\zeta^{CS}_{gen} + F^*_{gen}\right\}, \tag{22}$$

where the supra-index CS denotes values computed from the computation sequence. To avoid ζ_{gen} differentiation, the residual generator is implemented based on Sundström et al. (2013) as

$$\dot{\zeta}_1 = -\lambda_1\zeta_1 - \lambda_1^2\zeta_{gen}^{CS} + \lambda_1\frac{1}{\tau_{gen}}\left\{-\zeta_{gen}^{CS} + F_{gen}^*\right\}, \quad (23)$$

$$r_1 = \zeta_1 + \lambda_1\zeta_{gen}^{CS}, \quad (24)$$

with $\lambda_1 > 0$. This residual generator is equivalent to processing a relation obtained from (22) with a first-order low pass filter with unit DC gain and time constant $1/\lambda_1$.

- r_2: By choosing c_2 as the consistency relation, the computation sequence for r_2 is

$$\begin{aligned} CS_4 =&\{(m_1, x), (m_2, v), (m_4, F_w), (c_9, F_{WB}^{UP}), \\ &(c_{10}, F_{WB}^{DW}), (c_8, F_b), (c_4, p_{HS}), (c_5, p_n), \\ &(c_7, h_w), (c_6, p_a), (c_3, F_k), \\ &(\{c_{11}, c_{12}, d_3\}, \{\zeta_{gen}, \dot{\zeta}_{gen}, F_{gen}\})\}, \end{aligned} \quad (25)$$

and the ARR is given by

$$\dot{v} = \frac{1}{m_t}\left\{F_k^{CS} + F_b^{CS} + F_{gen}^{CS} + F_w^{CS}\right\}. \quad (26)$$

Thus, the residual generator, with $\lambda_2 > 0$, is

$$\dot{\zeta}_2 = -\lambda_2\zeta_2 - \lambda_2^2 y_2 + \frac{\lambda_2}{m_t}\left\{F_k^{CS} + F_b^{CS} + F_{gen}^{CS} + y_4\right\}, \quad (27)$$

$$r_2 = 25\{\zeta_2 + \lambda_2 y_2\}. \quad (28)$$

- r_3: By choosing c_1 as the consistency relation for r_3, the computation sequence is defined by x and v measurements. Thus, the ARR is defined by

$$\dot{x} = y_2, \quad (29)$$

and the residual generator, with $\lambda_3 > 0$, is

$$\dot{\zeta}_3 = -\lambda_3\zeta_3 - \lambda_3^2 y_1 - \lambda_3 y_2, \quad (30)$$

$$r_3 = 200\{\zeta_3 + \lambda_3 y_1\}. \quad (31)$$

5. SIMULATION TESTS

WEC simulations with selected faults were performed in MATLAB/Simulink for testing the reliability of the SA and the residual generators. Irregular sea waves were modeled by approximating the JONSWAP spectrum (Gieske, 2007). Parameter values are taken from Prado et al. (2006) and Gieske (2007), but p_a^0, p_n^0, and h_w are assumed so that $x^0 = 0$ and the floater natural oscillation period $T_n = 10$ s. Residual generators are implemented with $\lambda_{1,2,3} = 10$. Operation of the WEC within 1400 s is considered, and the following faults were included.

- f_1 : 10% x sensor gain reduction for $t \in [100, 200]$.
- f_2 : 10% v sensor gain reduction for $t \in [300, 400]$.
- f_3 : 50% LPMG gain reduction for $t \in [500, 600]$.
- f_4 : 40% F_{WB}^{UP} damping reduction for $t \in [700, 800]$.
- f_5 : 40% F_{WB}^{DW} damping reduction for $t \in [900, 1000]$.
- f_6: produced by 0.05 m diameter central tank perforation during $t \in [1100, 1150]$.

Residuals transient responses during active faults are presented in Figure 3.

From the residuals during the faults, the following observations are established:

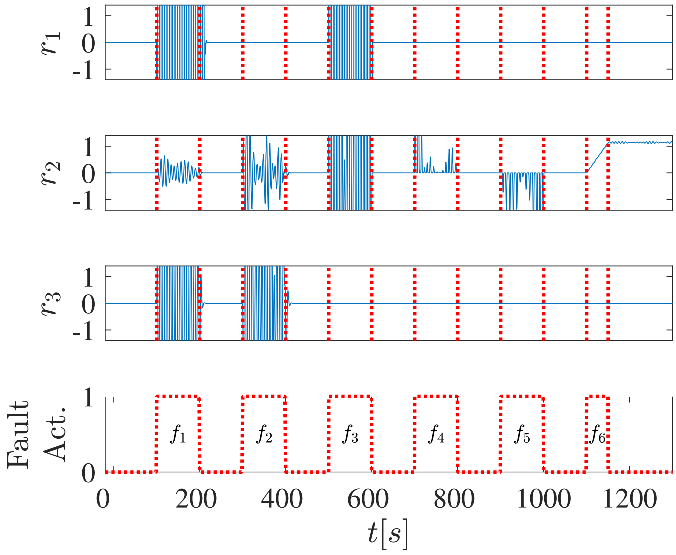

Fig. 3. Residuals transient response to faults

- All faults are detectable as established in Table 4.
- The fault f_6 affects the residual r_2, even if the fault is deactivated. This is justified because the additional water does not disappear even if the perforation is repaired.
- The effects of faults f_4 and f_5 have opposite signs. This fact could be used to isolate both faults in spite of the SA results.
- The f_6 effect over r_2 is noticeable in its mean value, and unlike the other faults, it does not introduce oscillations in the transient response.

Considering the mentioned observations, f_4, f_5, and f_6 could be isolated by processing r_2. This allows proposing the following residuals derived from r_2:

$$r_2^+ = r_2 H(r_2), \quad (32)$$

$$r_2^- = -r_2 H(-r_2), \quad (33)$$

$$r_2^f = \frac{d}{dt} r_2, \quad (34)$$

where r_2^+ and r_2^- are the positive and negative values of r_2, and r_2^f is obtained by differentiating r_2 in order to filter out the f_6 effect over r_2.

Simulation results of the added residuals are presented in Figure 4.

Observed results demonstrate that f_4, f_5, and f_6 could be isolated by processing r_2. This allows establishing the "extended fault signature matrix" presented in Table 5.

Table 5. Extended Fault Signature Matrix

	f_1	f_2	f_3	f_4	f_5	f_6
r_1	•		•			
r_2	•	•	•	•	•	•
r_3	•	•				
r_2^+	•	•	•	•		•
r_2^-	•	•	•		•	
r_2^f	•	•	•	•	•	

6. CONCLUSIONS

From structural analysis of a complex large-scale wave energy converter, structural detectability and isolability of

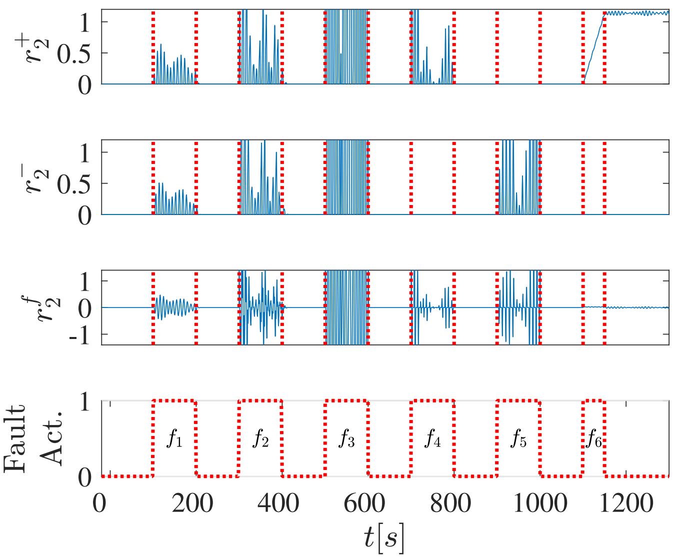

Fig. 4. Added residuals transient response to faults

some faults have been determined, and structured residuals have been designed. Numeric simulations of the system allowed to evaluate the performance of the designed structured residuals. Obtained results have demonstrated structural properties of the studied faults established from the analysis. In addition, it has been seen that faults over upper and lower water brakes produce opposite sign effects. By considering this fact, new residuals were derived. These derived residuals allowed achieving the isolation of upper and lower water brakes faults. Likewise, the tank perforation effect has been also isolated by differentiating one of the original residuals. Even though the results are satisfactory enough, they could be improved by considering a threshold adjustment for each residual.

REFERENCES

Ambühl, S., Marquis, L., Kofoed, J.P., and Dalsgaard Sørensen, J. (2015). Operation and maintenance strategies for wave energy converters. *Proceedings of the Institution of Mechanical Engineers, Part O: Journal of Risk and Reliability*, 229(5), 417–441.

Beirao, P. (2007). *Modelling and Control of a Wave Energy Converter: Archimedes Wave Swing*. Ph.D. thesis, Lisboa, Portugal.

Blanke, M., Kinnaert, M., Lunze, J., and Staroswiecki, M. (2016). *Diagnosis and Fault-Tolerant Control*. Springer-Verlag.

Chandrasekaran, S. and Raghavi, B. (2015). Design, Development and Experimentation of Deep Ocean Wave Energy Converter System. *Energy Procedia*, 79, 634 – 640. 2015 International Conference on Alternative Energy in Developing Countries and Emerging Economies.

Drew, B., Plummer, A.R., and Sahinkaya, M.N. (2009). A review of wave energy converter technology. *Proceedings of the Institution of Mechanical Engineers, Part A: Journal of Power and Energy*, 223(8), 887–902.

Dulmage, A.L. and Mendelsohn, N.S. (1958). Coverings of bipartite graphs. *Canadian Journal of Mathematics*, 10, 517–534.

Falnes, J. (2002). *Ocean Waves and Oscillating Systems: Linear Interaction including Wave-Energy Extraction*. Cambridge University Press.

Gieske, P. (2007). *Model Predictive Control of a Wave Energy Converter: Archimedes Wave Swing*. Master's thesis, Delft University of Technology, Delft, Netherlands.

Johanson, M., von Hacht, A., Strang-Moran, C., Hüffmeier, J., and Johannesson, P. (2019). Condition monitoring for wave energy converters. In *12th European Wave and Tidal Energy Conference (EWTEC 2019), Naples, September 1-6, 2019*.

Krysander, M., Åslund, J., and Nyberg, M. (2007). An efficient algorithm for finding minimal overconstrained subsystems for model-based diagnosis. *IEEE Transactions on Systems, Man, and Cybernetics-Part A: Systems and Humans*, 38(1), 197–206.

Liu, H. and Yu, L. (2017). Analytical method of fault detection and isolation based on bond graph for electromechanical actuator. In *2017 IEEE International Conference on Mechatronics and Automation (ICMA)*, 393–397.

Magagna, D. and Uihlein, A. (2015). Ocean energy development in europe: Current status and future perspectives. *International Journal of Marine Energy*, 11, 84 – 104.

Mork, G., Barstow, S., Kabuth, A., and Pontes, M. (2010). Assessing the global wave energy potential. In *ASME. International Conference on Offshore Mechanics and Arctic Engineering. 29th International Conference on Ocean, Offshore and Arctic Engineering*, volume 3, 447–454.

Pecher, A. and Kofoed, J.P. (2017). *Handbook of Ocean Wave Energy*. Springer International Publishing.

Penalba, M., Giorgi, G., and Ringwood (2017). Mathematical modelling of wave energy converters: A review of nonlinear approaches. *Renewable and Sustainable Energy Reviews*, 78, 1188–1207.

Prado, M., Gardner, F., Damen, M., and Polinder, H. (2006). Modelling and test results of the Archimedes Wave Swing. *Proceedings of The Institution of Mechanical Engineers Part A-journal of Power and Energy - PROC INST MECH ENG A-J POWER*, 220, 855–868.

Staroswiecki, M., Cassar, J.P., and Declerck, P. (2000). A structural framework for the design of fdi system in large scale industrial plants. In *Issues of fault diagnosis for dynamic systems*, 245–283. Springer.

Sundström, C., Frisk, E., and Nielsen, L. (2013). Selecting and utilizing sequential residual generators in fdi applied to hybrid vehicles. *IEEE Transactions on Systems, Man, and Cybernetics: Systems*, 44(2), 172–185.

Wolf, H. (2013). Structural analysis toolbox.

Wu, F., Ju, P., Zhang, X., Qin, C., Peng, G.J., Huang, H., and Fang, J. (2013). Modeling, control strategy, and power conditioning for direct-drive wave energy conversion to operate with power grid. *Proceedings of the IEEE*, 101(4), 925–941.

Zhang, J. and Rizzoni, G. (2014). Structural analysis for fdi of pmsm drive system in electric vehicles. In *2014 IEEE Conference and Expo Transportation Electrification Asia-Pacific (ITEC Asia-Pacific)*, 1–7. IEEE.